Progress In Electromagnetics Research M, Vol. 77, 41–50, 2019

A Contactless Electromagnetic Coupling Resonance-Based Volume Fraction Detection Technique for Gas-Liquid Flow

Yanyan Shi[1], Xiaolei Sun[1], Can Wang[1], Minghui Shen[2], and Meng Wang[1, *]

Abstract—To obtain the volume fraction of a gas-liquid two-phase flow, a contactless electromagnetic coupling resonance based volume fraction detection (CECR-VFD) technique is proposed. By mathematical calculation and numerical simulation, it is found that the CECR-VFD method is a better alternative than the conventional electromagnetic induction based method. The distance between the excitation coil and receiving coil is firstly determined. Then the effect of the pipe length is investigated. Additionally, the relationship between the output voltage across the receiving coil and the volume fraction is studied for stratified flow and annular flow. Experiments have been carried out for validation, and the results indicate that the output voltage can be used to predict the volume fraction of a two-phase flow.

1. INTRODUCTION

Description, explanation and measurement of two-phase flow are necessary and required in a variety of industrial applications such as chemical reaction, pipeline transportation and medical treatment [1–3]. Simultaneous flow of gas and liquid, which is termed as gas-liquid two-phase flow, is commonly encountered. In a gas-liquid flow, the determination of the volume fraction is of significant importance as it is essential to characterize flow behavior and fundamental to predict transfers of mass, momentum and energy [4–7].

Nowadays, there are numerous measurement techniques to obtain the volume fraction of the two-phase flow. Based on the difference of electrical characteristics between liquid and gas, it can be generally divided into two measurement methods, namely a conductive method [8–10] and a capacitance method [11–13]. The conductive method is suitable for measurements of the volume fraction in a gas-liquid flow where the continuous phase is conductive, while the capacitance method is preferred in parameter measurements in non-conductive two-phase flows. In addition, based on the law of electromagnetic induction, the electromagnetic tomography (EMT) has become a recognized and well established technique to obtain the physical parameters of complex two-phase flows without the requirement of physical contact [14–17]. For example, the two-phase flow with low conductivity is analyzed in [18] with 16 coils (8 transmitters and 8 receivers) and the reconstructed images from the real sample experiments are provided and discussed. In another case, experiments are conducted for the two-phase flow covering a broad range of conductivity contrasts and the capability of the EMT system in conductive phase imaging is demonstrated [19]. Furthermore, a new methodology is presented in [20] for identifying three different flow regimes (annular, stratified and bubbly), and the volume fraction of a gas-liquid flow with different densities is estimated [20]. In the literature, vortex signal of a stratified two-phase flow in a horizontal pipe had been discussed in atmospheric conditions, and the relationship between the void fraction and the relative amplitude spectrum of a two-phase flow is obtained [21].

Received 25 September 2018, Accepted 6 December 2018, Scheduled 14 December 2018

* Corresponding author: Meng Wang (wangmeng@htu.edu.cn).

[1] College of Electronic and Electrical Engineering, Henan Normal University, Xinxiang, Henan 453007, China. [2] Xinxiang Power Supply Company, State Grid Corporation of China, Xinxiang 453000, China.

However, the eddy current induced voltage signal is generally very small, and it is very necessary to increase the measured voltage for an accurate measurement.

In this paper, a contactless electromagnetic coupling resonance-based volume fraction detection (CECR-VFD) technique is proposed to measure the volume fraction of gas-liquid flow. The basic measurement principle and the equivalent circuit model are presented. The performance of the CECR-VFD technique is studied and compared with that of electromagnetic induction. The relationship between the measured voltage and volume fraction is investigated for stratified flow and annular flow by simulation. An experimental prototype is established and static experiments are performed for validation.

2. THEORETICAL FOUNDATION OF PROPOSED CECR-VFD METHOD

In a time-varying magnetic field, eddy currents occur in the gas-liquid flow where the continuous phase is conductive. With a variation of the volume fraction, the eddy current loss varies. Fig. 1 shows the diagram of the volume fraction measurement method based on the magnetic coupling between two coils. It is mainly composed of an excitation coil which is connected to a power source with an alternating exciting frequency, a pipe filled with gas and water, and a detection coil linked with a load. For a fixed distance between the excitation coil and the detection coil when there is no detected object, the measured voltage across the load is fixed. However, once a pipe is positioned inside the coils, the load voltage varies due to the eddy current loss when the distribution of gas and water changes. Therefore, there is a relationship between the variation of the output voltage and the volume fraction. The turns of the excitation coil and the detection coil are considered as N_1, N_2. The radius of the coil and pipe are denoted as r_1, r_2 respectively. The distance between the excitation coil and detection coil is denoted as D. The length of the pipe is denoted as L.

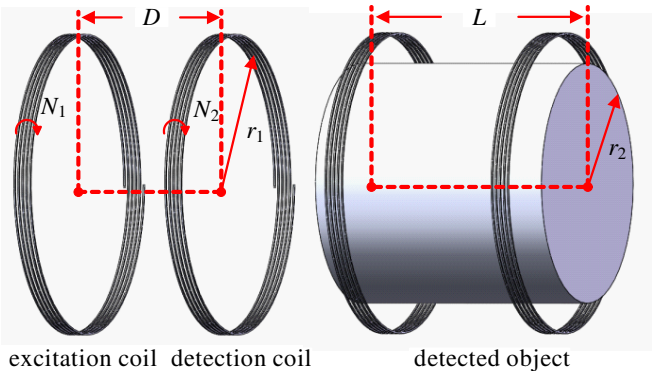

Figure 1. Diagram of volume fraction measurement method.

Figure 2 shows the equivalent circuit of the volume fraction detection system based on electromagnetic induction. The resistance of the power source is denoted as R_S. The excitation coil and the detection coil can be modeled as a serial connection of self-inductance and resistance (L_1, R_1 and L_2, R_2 respectively). The pipe filled with gas and water is considered as R_3 and L_3. I_{1i} ($i = 1, 2, 3$) is the current flowing in the loops, and M_{1i} is the mutual inductance among loops. The resistance R_L is the load resistance.

From Kirchhoff's law, the equivalent circuit can be expressed as

$$\begin{aligned} V_S &= (R_1 + R_S + j\omega L_1)I_{11} - j\omega M_{12}I_{12} - j\omega M_{13}I_{13} \\ 0 &= -j\omega M_{12}I_{11} + (R_2 + R_L + j\omega L_2)I_{12} + j\omega M_{23}I_{13} \\ 0 &= -j\omega M_{13}I_{11} + j\omega M_{23}I_{12} + (R_3 + j\omega L_2)I_{13} \end{aligned} \tag{1}$$

where ω is the angular frequency of the power source.

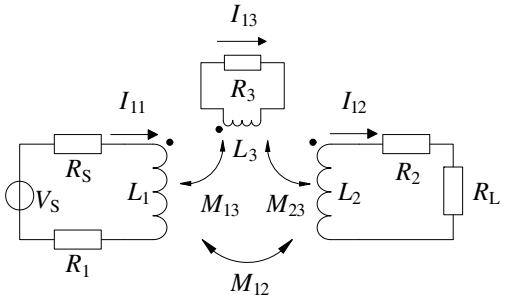

Figure 2. Equivalent circuit of the electromagnetic induction mode.

Based on Eq. (1), the load voltage V_L across the detection coil can be calculated as

$$V_L = I_{12}R_L = \frac{D_{12}}{D_{11}}R_L \tag{2}$$

where

$$\begin{aligned} D_{11} &= \begin{vmatrix} R_1 + R_S + j\omega L_1 & -j\omega M_{12} & -j\omega M_{13} \\ -j\omega M_{12} & R_2 + R_L + j\omega L_2 & j\omega M_{23} \\ -j\omega M_{13} & j\omega M_{23} & R_3 + j\omega L_3 \end{vmatrix} \\ D_{12} &= \begin{vmatrix} R_1 + R_S + j\omega L_1 & V_S & -j\omega M_{13} \\ -j\omega M_{12} & 0 & j\omega M_{23} \\ -j\omega M_{13} & 0 & R_3 + j\omega L_2 \end{vmatrix} \end{aligned} \tag{3}$$

In the traditional electromagnetic induction-based volume fraction detection system, the coupling effect between the excitation coil and the detection coil is relatively weak, and a small load voltage is measured.

To solve the problem above, a volume fraction detection method based on electromagnetic coupling resonance is proposed. Fig. 3 is the equivalent schematic diagram of the CECR-VFD. The electrical parameters of the circuit are identical to that in Fig. 2. However, a capacitance (C_1, C_2) is introduced in the excitation and detection circuit for magnetic resonance and maximum power transfer.

For the power source with the angular frequency of ω, the compensated capacitance can be calculated as

$$\begin{aligned} C_1 &= \frac{1}{\omega^2 L_1} \\ C_2 &= \frac{1}{\omega^2 L_2} \end{aligned} \tag{4}$$

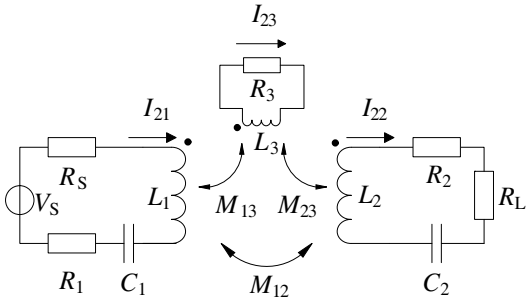

Figure 3. Equivalent schematic diagram of CECR-VFD.

According to Kirchhoff's law, it can be obtained as

$$\begin{aligned} V_S &= (R_1 + R_S)I_{21} - j\omega M_{12}I_{22} - j\omega M_{13}I_{23} \\ 0 &= -j\omega M_{12}I_{21} + (R_2 + R_L)I_{22} + j\omega M_{23}I_{23} \\ 0 &= -j\omega M_{13}I_{21} + j\omega M_{23}I_{22} + (R_3 + j\omega L_3)I_{23} \end{aligned} \tag{5}$$

Based on Eq. (5), the output voltage U_L across the load is calculated as

$$U_L = I_{22}R_L = \frac{D_{22}}{D_{21}}R_L \tag{6}$$

where

$$\begin{aligned} D_{21} &= \begin{vmatrix} R_1 + R_S & -j\omega M_{12} & -j\omega M_{13} \\ -j\omega M_{12} & R_2 + R_L & j\omega M_{23} \\ -j\omega M_{13} & j\omega M_{23} & R_3 + j\omega L_3 \end{vmatrix} \\ D_{22} &= \begin{vmatrix} R_1 + R_S & V_S & -j\omega M_{13} \\ -j\omega M_{12} & 0 & j\omega M_{23} \\ -j\omega M_{13} & 0 & R_3 + j\omega L_3 \end{vmatrix} \end{aligned} \tag{7}$$

Comparing Eq. (2) and Eq. (6), it can be obtained that

$$\frac{U_L}{V_L} = \frac{D_{22}}{D_{21}}\frac{D_{11}}{D_{12}} = \frac{D_{11}}{D_{21}} > 1 \tag{8}$$

It can be seen from Eq. (8) that the load voltage measured by the electromagnetic coupling resonant method is larger which will show better performance in the parameter estimation when the voltage is very small or noise exists in the measurement. As a result, more power can be delivered to the load and less energy is consumed when the load voltage is measured by the electromagnetic coupling resonant method.

3. SIMULATION ANALYSES

3.1. Determination of Distance between Coils and Pipe Length

Based on the above theoretical analysis, simulation work is carried out by ANSYS MAXWELL. The system model is established by using the field-circuit coupling finite element method. The simulation parameters are shown in Table 1.

Table 1. Parameters of CECR-VFD system.

Parameters	Value
Radius of the coils	100 mm
Number of turns of the coils	5
Resistance of source and load	50 Ω
Source voltage	3.5 V
Resonant frequency	4 MHz

The distance between the two coils needs to be studied first. Fig. 4 shows the variation of the load voltage against the transfer distance based on the two methods. It can be seen that the load voltage obtained with the electromagnetic coupling resonance is higher than that with the electromagnetic induction. The inductive voltage shows a continuous downward trend with the increase of distance. However, the resonant voltage increases first and then decreases. This is because when the distance between the coils drops below a certain value, a frequency splitting occurs due to the magnetic over-coupling which leads to the decrease of the load voltage. For maximum power transfer, the distance between the coils is set to 60 mm where the output voltage is the highest.

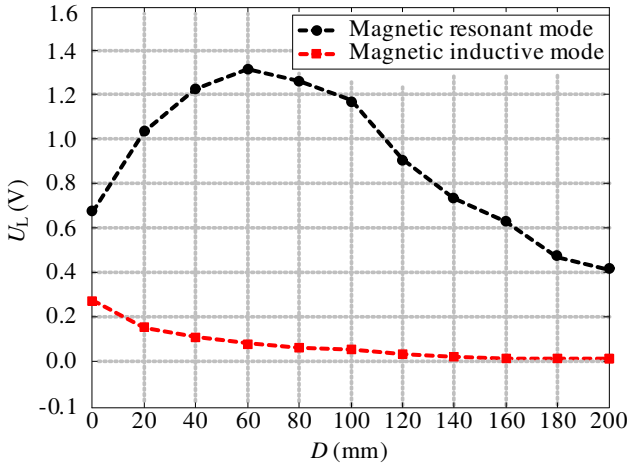

Figure 4. Comparison of the load voltage obtained with the two methods.

The length of the pipe is also a critical element that affects the power transfer. In the simulation, the pipeline is filled with liquid and the conductivity is set to 0.3 s/m. Fig. 5 shows how the eddy current loss and eddy current changes with the variation of the pipe length. It can be obtained that the eddy current loss and eddy current increase monotonically when the pipe is shorter than 300 mm, and then it tends to be constant when the pipe is longer than 300 mm which indicates that it can be viewed as an infinitely long pipe, and no effect is imposed on the measurement.

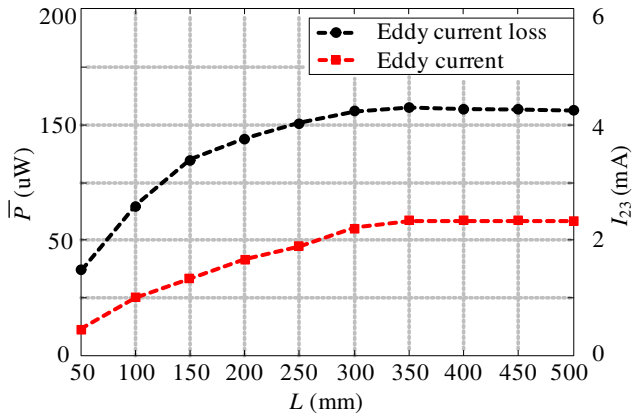

Figure 5. Variation of the eddy current loss and eddy current against the pipe length.

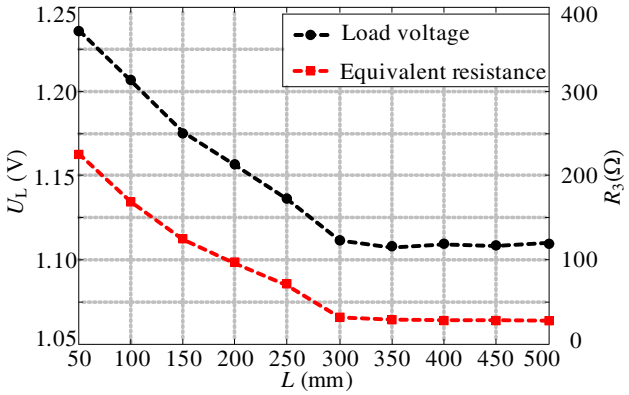

Figure 6. Relationship between the equivalent resistance and the load voltage.

Based on the average eddy current loss and effective current value, the equivalent resistance of the measured object can be obtained. Fig. 6 shows the load voltage and the equivalent resistance of the measured object. It can be seen that the load voltage and equivalent resistance decrease firstly with the increase of the pipe length due to eddy current loss. Nevertheless, it keeps constant when the pipe is longer than 300 mm.

3.2. Characterization of the Volume Fraction

In a gas-liquid two-phase flow, stratified flow and annular flow are two frequently encountered flow regimes. The schematic of the flow patterns are illustrated in Fig. 7.

For stratified flow, the height of the liquid is denoted as H. Therefore, the volume fraction of the

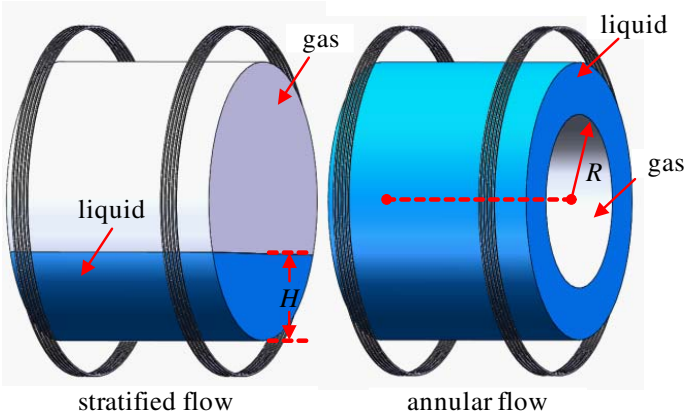

Figure 7. Stratified flow and annular flow.

liquid, α_1, can be calculated as

$$\begin{aligned}\alpha_1 &= \frac{r_2^2 \arccos\frac{r_2 - H}{r_2} - (r_2 - H)\sqrt{2r_2H - H^2}}{\pi r_2^2} \quad (H \le r_2) \\ \alpha_1 &= 1 - \frac{r_2^2 \arccos\frac{H - r_2}{r_2} - (H - r_2)\sqrt{2r_2H - H^2}}{\pi r_2^2} \quad (H > r_2)\end{aligned} \tag{9}$$

Figure 8 shows the equivalent resistance and inductance of the detected object and the mutual inductance variations versus the liquid volume fraction. It can be seen that the equivalent resistance decreases with the increase of the liquid volume fraction while the inductance tends to increase. The mutual inductance between the excitation coil (or detection coil) and the detected object increases when more liquid is injected. However, they are much smaller than the mutual inductance between the excitation coil and detection coil.

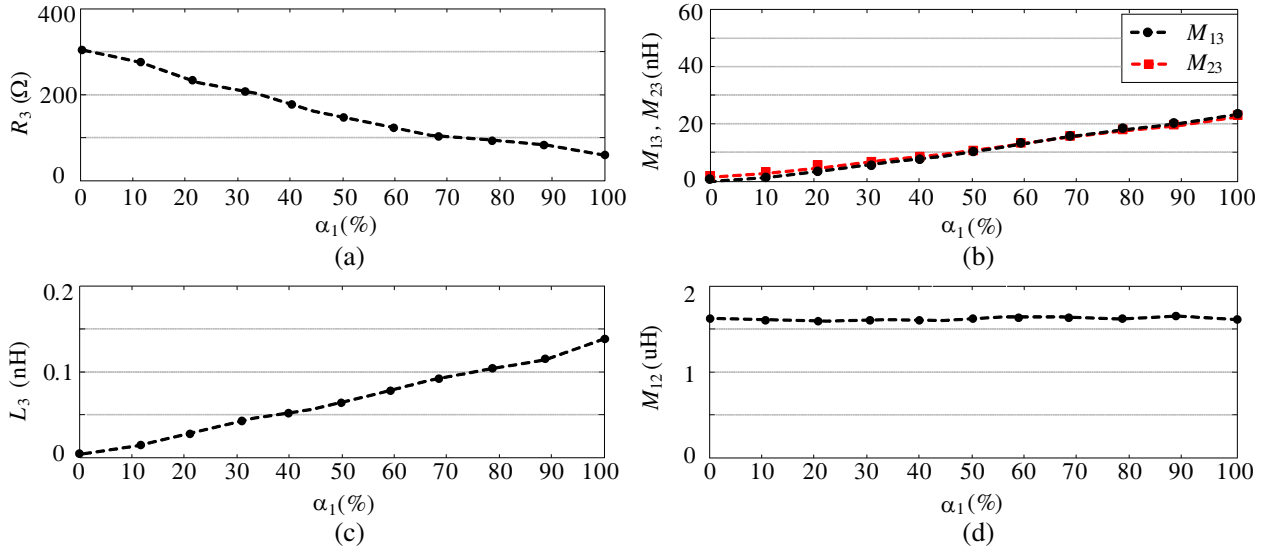

Figure 8. Variation of resistance and inductance along with the mutual inductance for the stratified flow. (a) Equivalent resistance. (b) Mutual inductance between the excitation coil (or detection coil) and the detected object. (c) Inductance of the stratified flow. (d) Mutual inductance between the excitation coil and detection coil.

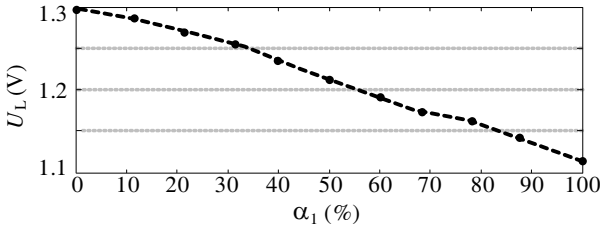

Figure 9. Variation of output voltage against liquid volume fraction for stratified flow.

Figure 9 shows the output voltage across the load against the liquid volume fraction. The load voltage decreases monotonically as more eddy current losses are caused with the increase of liquid level. The relationship between the output voltage and the liquid volume fraction for stratified flow can be represented as

$$U_L = -0.0016 \times \alpha_1 + 1.299 \tag{10}$$

For annular flow, the radius of the insulating plastic rods is denoted as R. The volume fraction of the liquid, α_2, can be calculated as

$$\alpha_2 = \frac{\pi \left(r_2^2 - R^2\right)}{\pi r_2^2} \tag{11}$$

The simulation results are shown in Fig. 10. The results for annular flow are very similar with that in stratified flow.

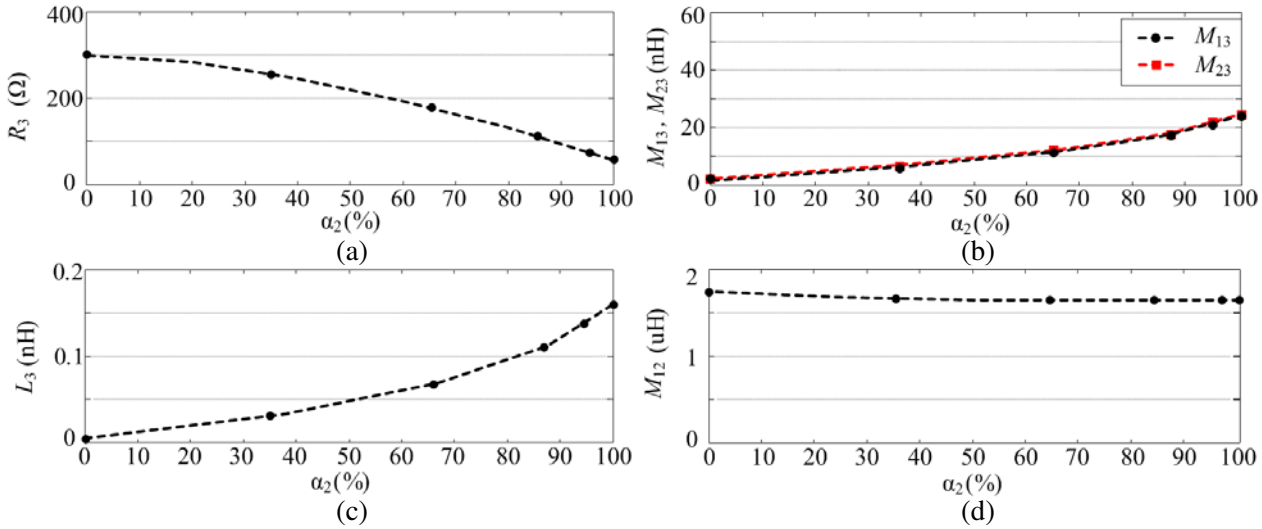

Figure 10. Variation of resistance and inductance along with the mutual inductance for the annular flow. (a) Equivalent resistance. (b) Mutual inductance between the excitation coil (or detection coil) and the detected object. (c) Inductance of the annular flow. (d) Mutual inductance between the excitation coil and detection coil.

Figure 11 is variation of output voltage versus liquid volume fraction for annular flow. The relationship between the output voltage, and the liquid volume fraction for annular flow can be expressed as

$$U'_L = -0.1178 \times \alpha_2^2 - 0.0271 \times \alpha_2 + 1.286 \tag{12}$$

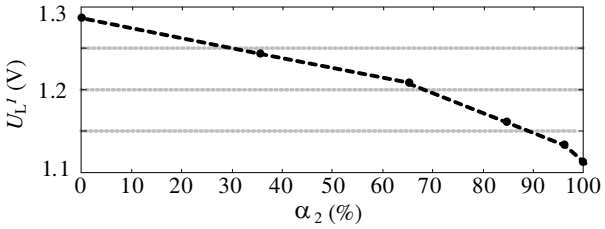

Figure 11. Variation of output voltage against liquid volume fraction for annular flow.

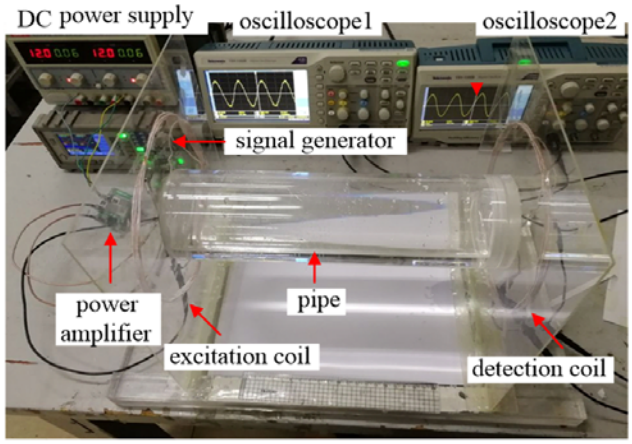

Figure 12. Experimental prototype.

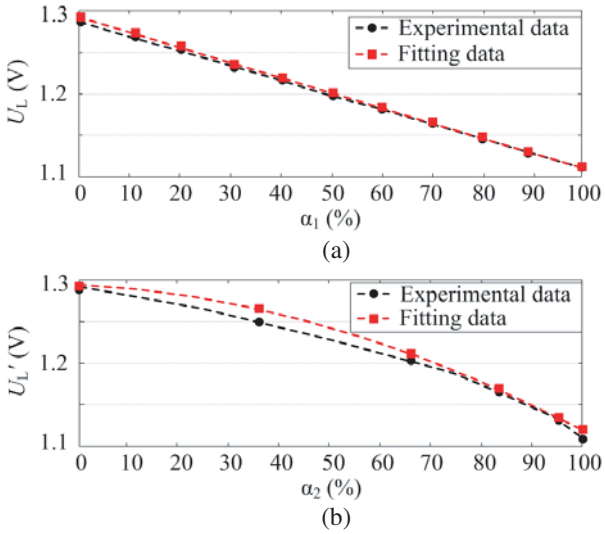

Figure 13. Measured voltage and calculated voltage for stratified flow and annular flow. (a) Stratified flow. (b) Annular flow.

4. EXPERIMENTAL VALIDATION

For validation, an experimental prototype is established, as shown in Fig. 12. In the static experiment, the system parameters are exactly the same as that in the simulation. The conductivity of liquid is set to 0.3 s/m. The excitation frequency of liquid is 4 MHz. According to the resonant frequency and measured inductance of the coils, the compensated capacitance can be calculated. The high-frequency

power amplifier BUF634 with 24 dB magnification is applied in the experiment. The excitation coil is connected to a signal generator via a power amplifier and the detection coil is linked with a load. For the stratified flow, the pipe is placed horizontally and liquid is injected into the pipe. For the annular flow, several insulating plastic rods with various diameters are supposed to be placed inside the pipe filled with conductive liquid.

Figure 13 shows the measured voltage and calculated voltage for stratified flow and annular flow. It can be observed that there exists good consistency between the measured and calculated values while the measured voltage is a little smaller than that obtained with the simulation. This may be attributed to the external electromagnetic disturbance and the measurement error.

5. CONCLUSION

In this paper, a CECR-VFD technique is proposed. The circuit model is analyzed for the new method and compared with the traditional inductive mode. The mathematical calculation and finite element analysis indicate that the output voltage across the detection coil is much larger for the CECR-VFD. The effect of the pipe is studied and it is found that it should be longer than 300 mm when its impact can be neglected. The variation of equivalent resistance and inductance against the volume fraction are investigated for the stratified flow and annular flow. Besides, the relationship between the load voltage and the volume fraction of the stratified flow and annular flow is obtained. Static experiments are carried out, and experimental results are compared with calculations. The results demonstrate that the load voltage obtained with the CECR-VFD technique can be applied to estimate the volume fraction in typical gas-liquid flow.

ACKNOWLEDGMENT

This work was supported by the National Natural Science Foundation of China under Grant 61640303, the Key Science and Technology Project of Henan Province of China under Grant No. 182102210080 and the Foundation for University Key Young Teacher by Henan Province of China under Grant No. 2017GGJS040.

REFERENCES

1. Thorn, R., G. A. Johansen, and B. T. Hjertaker, "Three-phase flow measurement in the petroleum industry," *Measurement Science and Technology*, Vol. 24, No. 1, 1–17, 2013.
2. Figueiredo, M. M. F., J. L. Goncalves, A. M. V. Nakashima, and R. D. M. Carvalho, "The use of an ultrasonic technique and neural networks for identification of the flow pattern and measurement of the gas volume fraction in multiphase flows," *Experimental Thermal and Fluid Science*, Vol. 70, 29–50, 2016.
3. Franco Jr., E. F., R. M. Salgado, and T. Ohishi, "Analysis of two-phase flow pattern identification methodologies for embedded systems," *IEEE Latin America Transactions*, Vol. 16, No. 3, 718–727, 2018.
4. Xie, S. W., J. Z. Gao, and Z. T. Wen, "The optimal design of the new tube inside and outside differential pressure flow meter," *Applied Mechanics and Materials*, Vol. 541, No. 7, 1283–1287, 2014.
5. Ghanei, S., M. Kashefi, and M. Mazinani, "Eddy current nondestructive evaluation of dual phase steel," *Materials & Design*, Vol. 50, No. 17, 491–496, 2013.
6. Al-Naser, M., M. Elshafei, and A. M. Al-Sarkhi, "Artificial neural network application for multiphase flow patterns detection: A new approach," *Journal of Petroleum Science and Engineering*, Vol. 145, 548–564, 2016.
7. Sun, H. J., Z. J. Liu, and L. F. Wang, "Research on the installation location of the vortex probe for gas-liquid two-phase flow with low liquid fraction," *Journal of Mechanical Engineering*, Vol. 50, No. 4, 167–171, 2014.

8. Gao, Z., Y. Yang, L. Zhai, N. Jin, and G. Chen, "A four-sector conductance method for measuring and characterizing low-velocity oil-water two-phase flows," *IEEE Transactions on Instrumentation & Measurement*, Vol. 65, No. 7, 1690–1697, 2016.
9. Faraj, Y., M. Wang, and J. Jia, "Automated horizontal slurry flow regime recognition using statistical analysis of the ERT signal," *Procedia Engineering*, Vol. 102, 821–830, 2015.
10. Wang, H. G., G. R. Zhao, and G. Z. Qiu, "Investigation the solid phase distribution in the inlet of multi-cyclone of a circulating fluidized bed by electrical capacitance tomography," *Journal of Engineering Thermophysics*, Vol. 35, No. 1, 109–113, 2014.
11. Madhavi, S., H. Sagar, and R. Vivek, "Void fraction measurement using electrical capacitance tomography and high speed photography," *Chemical Engineering Research and Design*, Vol. 94, 1–11, 2015.
12. Yang, D. Y., R. Guo, and X. R. Wang, "Application of electrical capacitance tomography on lubricating oil film in journal bearings," *Proceedings of the CSEE*, Vol. 32, No. 5, 187–190, 2012.
13. Hamidipour, A., T. Henriksson, and M. Hopfer, "Electromagnetic tomography for brain imaging and stroke diagnostics: Progress towards clinical application," *Cells Tissues Organs*, Vol. 166, No. 2, 233–246, 2018.
14. Liu, Z. W. Li, and F. Xue, "Electromagnetic tomography rail defect inspection," *IEEE Transactions on Magnetics*, Vol. 51, No. 10, 1–7, 2015.
15. Mayank, G., M. Prabhat, K. Ashok, and S. Anupam, "Nonuniform arrangement of emitter-receiver pairs arrangement and compact ultrasonic tomography setup," *IEEE Sensors Journal*, Vol. 15, No. 2, 1198–1207, 2014.
16. Fu, Y., C. Tan, and F. Dong, "Analysis of response for magnetic induction tomography with internal source," *Measurement*, Vol. 78, No. 1, 260–277, 2016.
17. Dekdouk, B., C. Ktistis, and D. W. Armitage, "Absolute imaging of low conductivity material distributions using nonlinear reconstruction methods in magnetic induction tomography," *Progress in Electromagnetics Research*, Vol. 155, 1–18, 2016.
18. Wei, H. Y. and M. Soleimani, "Two-phase low conductivity flow imaging using magnetic induction tomography," *Progress in Electromagnetics Research*, Vol. 131, No. 20, 99–115, 2012.
19. Lu, M., H. Andy, and S. Manuchehr, "Experimental evaluation of conductive flow imaging using magnetic induction tomography," *International Journal of Multiphase Flow*, Vol. 72, No. 20, 198–209, 2015.
20. Roshani, G. H., E. Nazemi, and M. M. Roshani, "Identification of flow regime and estimation of volume fraction independent of liquid phase density in gas-liquid two-phase flow," *Progress in Nuclear Energy*, Vol. 98, 29–37, 2017.
21. Zhang, J. and T. Zhang, "Research on signal amplitude of the Kármán vortex street in gas-liquid two-phase flow with high void fraction," *Flow Measurement & Instrumentation*, Vol. 41, 158–164, 2015.